Rev.Adv.Mater.Sci. 10 (2005) 21-27

MULTI-SCALE MODELING OF TITANIUM DIOXIDE: CONTROLLING SHAPE WITH SURFACE CHEMISTRY

Amanda Barnard[1,2], Zoran Saponjic[3], David Tiede[1,3], Tijana Rajh[1,3] and Larry Curtiss[2,3]

[1]Center for Nanoscale Materials, Argonne National Laboratory, Argonne, IL 60439, USA
[2]Materials Science Division, Argonne National Laboratory, Argonne, IL 60439, USA
[3]Chemistry Division, Argonne National Laboratory, Argonne, IL 60439, USA

Received: April 15, 2005

Abstract. An important aspect in the use of titanium dioxide at the nanoscale for advanced photochemical applications is the controlled manipulation of the size, phase and morphology of the nanoparticles in solution. Solution pH is often used to alter such properties at the nanoscale. We have used a multi-scale thermodynamic model to investigate the effects of pH on the shape and phase stability of titanium dioxide nanoparticles. As input for the model, surface energies and surface tension of low index stoichiometric surfaces of anatase and rutile under hydrogen rich and hydrogen poor conditions have been calculated using density functional theory. Our results show how the anatase phase is stabilized in acidic solution while the rutile phase is stabilized in alkaline solution, and that pH may also be used to induce structural and phase transitions.

1. INTRODUCTION

The size, shape, and crystal structure of nanoparticles are important parameters that control their chemical, optical, and electrical properties and determine their catalytic activity [1-3]. The ability to systematically manipulate the size and shape of metal oxide nanoparticles is a major scientific breakthrough in opening new venues for development of materials capable of efficient photoinduced charge separation. The current interest in titanium dioxide nanoparticles for advanced photochemical applications [4] has prompted a number of studies to analyze the properties of titanium dioxide surfaces under various conditions, such as acids and bases [5,6]. TiO_2 nanoparticles are typically generated via sol-gel synthesis, and it has been known for some time that the pH value of the sol-gel is a decisive factor for controlling the final particle size [7], shape [8], phase[7,9,10] and agglomeration [11].

In the case of anatase (for example), it has been reported that synthesis under basic conditions results in small cubic-like nanocrystals with {112} and {103} facets [12], hexagonal nanocrystals [13], or short rod-like nanocrystals with {010}, {101} and {001} facets [5,13]. In contrast, acidic conditions have been reported to result almost exclusively in truncated tetragonal bipyramidal nanocrystals with {101}, {001} and {010} facets [12,14,15]. Further, it has been found that the growth rate of anatase is dependent on pH[16]; and that an excess dilution of the particle density during synthesis causes partial dissolution of TiO_2 nanocrystals [12] (or melting [11]),

Corresponding author: Amanda Barnard, e-mail: amanda.barnard@anl.gov

possibly resulting in 'spherical' nanoparticles. In each case the final nano-morphology is dependent upon the value of the pH, and hence the properties of the nanocrystals will be sensitive to the chemistry at the surfaces[16-18]. This sensitivity to pH is especially important when designing nanoparticles suitable for interfacing with organic molecules [19].

In the present study, the affect of surface chemistry on the phase stability of anatase and rutile nanocrystals is investigated, using a multi-scale thermodynamic model and surface properties calculated using first principles methods [20]. The surface conditions were previously modeled by varying the ratio of hydrogen to oxygen in a complete monolayer of adsorbates, to represent different degrees of surface acidity. Hydrogen–rich (or H–terminated) surfaces were used to represent moderately (or highly) acidic conditions, whereas hydrogen–poor (or O–terminated) surfaces were used to represent moderately (or highly) basic conditions. Using these representations, the dependence of the nanoscale anatase-to-rutile phase transition on surface chemistry has been determined, and the prospect of surface chemistry-induced phase transitions addressed.

2. THEORETICAL METHODOLOGY

As mentioned above, we have used a multi-scale thermodynamic model [21] based on the Gibbs free energy G_x^0 of a nanoparticle of material x (x = A for anatase, and x = R for rutile). The (truncated) version of the model used here is applicable only to particles over ~3 nm in diameter (since edge and corner effects have been ignored) so that G_x^0 is described by a sum of contributions from the particle bulk and surfaces such that,

$$G_x^0 = G_x^{bulk} + G_x^{surface}. \quad (1)$$

This is then further defined in terms of the surface energy γ_{xi} for each crystallographic surface i, weighted by the factors f_i, such that $\Sigma_i f_i = 1$. Hence,

$$G_x^0 = \Delta_f G_x^0 + \frac{M}{\rho_x}(1-e)\left[q\sum_i f_i\gamma_{xi}\right], \quad (2)$$

where $\Delta_f G_x^0$ is the standard free energy of formation of the bulk (macroscopic) material [22], M is the molar mass, ρ_x is the density and e is the volume dilation induced by the surface tension. In general, the surface to volume ratio q and the weighting factors f_i must be calculated explicitly for each shape and the facet therein. In this model the size dependence is introduced not only by the surface to volume ratio q, but also by the reduction of e as the crystal grows larger. Shape dependence is also introduced by q, as well as the weighted sums of the surface energies and the surface tensions [21].

It has previously been shown [21] that the Laplace–Young equation is suitable for approximating the volume dilation of faceted nanocrystals [21,23]. Therefore, the volume dilation due to the surface tension, with the compressibility $\beta = 1/B_0$ (previously calculated [23] by fitting to the Vinet equation of state [24]), is defined as:

$$e = \frac{2\beta\sigma_x}{R}. \quad (3)$$

Here, σ_x is obtained by summing over the (weighted) surface tensions of the crystallographic surfaces present on the nanocrystal,

$$\sigma_x = \sum_i f_i\sigma_{xi}, \quad (4)$$

where σ_{xi} is the surface tension of the particular crystallographic surface i of phase x.

As mentioned above, the surface energies and surface tensions have been calculated elsewhere [20], using density functional theory (DFT) within the generalized gradient approximation (GGA), with adsorbates representing acidic, neutral and alkaline conditions [20]. From experiment, it is known that the structure of surfaces are determined by acid–base equilibria involving TiOH surface hydroxyl groups [25-29]. Under neutral pH conditions, the surfaces are found to be terminated with water adsorbates (either as molecular H_2O or as dissociated OH^-+H^+) capping the undercoordinated surface sites [25, 26]. When in acidic solutions protonation occurs, with the (lowest pH) limiting case occurring when all under-coordinated surface sites are protonated. Similarly, when in basic solution, the surfaces are deprotonated [28, 30], and the (upper pH) limiting case involves total deprotonation and all under-coordinated surface sites terminated with O.

Therefore, the surface acidity is primarily described by the ratio of H and O on the surface. In reference [20] such variations in surface chemistry were introduced by varying the ratio of hydrogen to oxygen in a complete monolayer of adsorbates, thereby representing different degrees of surface acidity. In this previous work, fully hydrogenated (H–terminated) surfaces were used to represent highly acidic surfaces; hydrogen–rich (with respect to H_2O terminations) surfaces were used to represent moderately acidic surfaces; hydrated (H_2O–terminated) surfaces were used to represent neutral surfaces;

hydrogen–poor (with respect to H_2O terminations) surfaces were used to represent moderately alkaline surfaces; and oxygenated (O–terminated) surfaces were used to represent highly alkaline surfaces. The respective chemical potentials were then constructed with respect to the neutral (hydrated) surfaces, and (as mentioned above) the surface energies and surface tensions calculated using DFT GGA. More details and final values γ_{xi} and σ_{xi} (for the anatase (001), (100), and (101) surfaces, and rutile (100), (110) and (011) surfaces) are contained within reference [20].

3. DEPENDENCE OF THE ANATASE–TO–RUTILE PHASE TRANSITIONS ON SURFACE CHEMISTRY

Using the appropriate γ_{xi} and σ_{xi} from reference [20], the value of G_A^0 and G_R^0 (from Eq. (2)) were calculated for anatase and rutile (respectively), and plotted together as a function of the number of TiO_2 units. These plots are shown in Figs. 1a–1e for each type of surface chemistry. The intersection points in each plot denotes the phase transition sizes, which have been conveniently converted to the equivalent average anatase nanoparticle diameter [31].

As shown in Fig. 1, the phase transitions for TiO_2 nanoparticles with hydrogenated, hydrogen–rich, hydrated, hydrogen–poor and oxygenated surfaces occur at sizes of approximately 22.7, 18.4, 15.1, 13.2, and 6.9 nm, respectively. This is not to say that anatase nanoparticle may not exist above these sizes, but it does indicate that above these sizes they will be metastable with respect to transformation to rutile. These results clearly demonstrate a dependence of the phase transition size on composition of the adsorbates. The anatase nanoparticles are stabilized by surface adsorbates containing a large fraction of hydrogen, whereas rutile nanoparticles are stabilized by surface adsorbates containing a large fraction of oxygen.

3.1. Phase transitions induced by changes in surface chemistry

Careful consideration of the results contained within Fig. 1 reveals another interesting result. A consequence of the dependence of the anatase–to–rutile phase transition on the surface chemistry is that the possibility is introduced for phase transitions to be induced by a change in the absorbed groups on the surfaces [31].

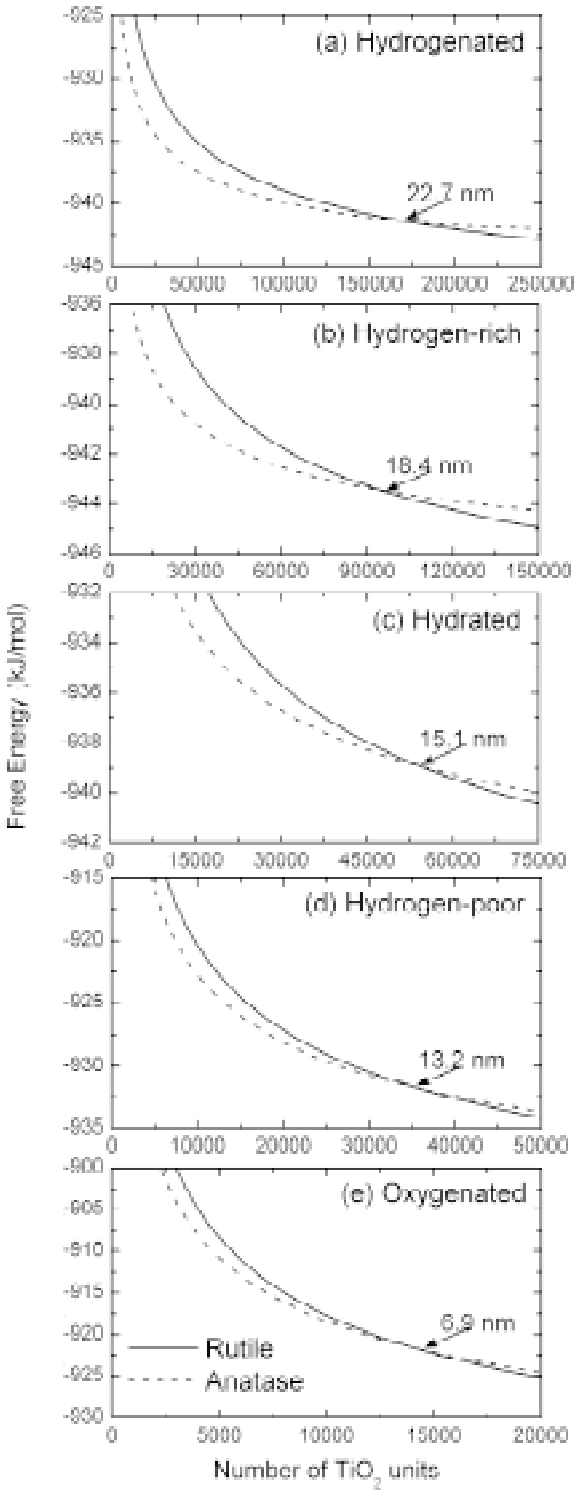

Fig. 1. Free energy as a function of number of TiO_2 units for anatase and rutile (a) with hydrogenated surfaces (b) with hydrogen–rich surface adsorbates, (c) hydrated surfaces, (d) hydrogen–poor adsorbates, and (e) oxygenated surfaces, calculated using the values of γ_{xi} and σ_{xi} from reference [20]. The intersection points indicate the phase transitions.

Consider a particle of ~14 nm. Under hydrogen–rich conditions (moderately acidic surfaces) anatase is thermodynamically stable since it is smaller than the phase transition size of 18.4 nm. However, sufficient deprotonation will cause the surface chemistry to alter and eventually to correspond to hydrogen–poor conditions (moderately alkaline surfaces) and may induce a phase transition to rutile since the particle is larger than the phase transition size of 13.2 nm.

It is also interesting to note that if we consider the same scenario for a 17 nm particle, the phase transition may be expected earlier in the deprotonation process, when the surfaces are neutralized (hydrated). This is because a 17 nm particle of anatase (while smaller than the transition size of 18.4 nm under hydrogen–rich conditions) is larger than the transition size of 15.1 nm for the case of neutral hydrated surfaces.

4. REVERSIBLE pH INDUCED PHASE TRANSITIONS IN TiO_2 NANOTUBES

Recently, much effort has been directed towards obtaining TiO_2 nanotubes with large surface areas and enhanced photocatalytic activity. Good examples of large surface area TiO_2 structures are scrolled (multi-walled) nanotubes and nanosheets. Previously we have reported scrolled TiO_2 nanotubes synthesized by a hydrothermal method using a variety of different starting materials (such as molecular Ti(IV) alkoxide, TiO_2 colloids, and Degussa P25), in the proton deficient aqueous systems (10M NaOH). All of the starting materials used for synthesis led to the formation of nanotubes having the same diameter of 12 nm, however the increasing concentration of TiO_2 precursors from 0.1 to 0.5M resulted in the systematic change in the length of scrolled TiO_2 nanotubes (while their diameter remained the same) [32].

Using high resolution TEM and selected area electron diffraction the nanotubes were found to possess the anatase structure, and to be comprised of layers. Due to the large fraction (~40%) of undercoordinated surface (titanium) sites, these layers are scrolled into a high curvature nanotube. It was found that the walls of the scrolled nanotubes are composed of 5 layers, with a layer–layer distance of 0.9±0.1 nm, separated by a gap of 0.3 nm, and with an inner tube void of 3 nm [32].

Although these nanotubes were synthesized in alkaline solution, it was found that by charging the undercoordinated surface sites with protons or lithium ions, the nanotubes unscrolled; transforming into extended sheet-like nanostructures. Under these low pH conditions the single-layer sheets remain stable, despite the high surface-to-volume ratio. The inclusion of this example is pertinent here, since this unscrolling of the anatase nanotubes was accompanied by a phase transition, resulting in nanosheets with the rutile structure. Small angle X-ray scattering (SAXS) and wide angle X-ray scattering (WAXS) spectrum taken during the unscrolling process has evidenced the fast disappearance of the broad peaks that describe a wall structure of scrolled nanotubes, followed by the development of new sharp diffraction peaks indicative of the formation of a rutile crystalline structure [32]. As the process of unscrolling continues, the whole spectrum transforms into the diffraction pattern of a rutile crystalline structure [32]. This is shown in the combined SAXS/WAXS spectra of powdered samples given in Fig. 2, with solid vertical bars used to indicate the characteristic diffraction peak positions expected for bulk anatase (a(101) and a(004)) and rutile (r(110), r(101) and r(111)).

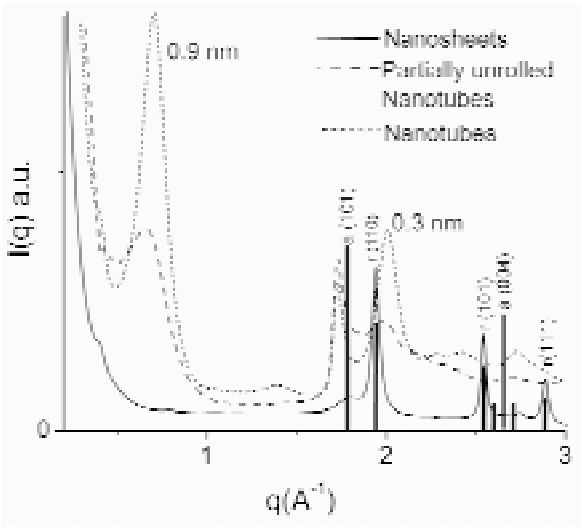

Fig. 2. Combined SAXS/WAXS spectra of powdered samples of anatase nanotubes, partially unscrolled TiO_2 nanotubes, and rutile nanosheets. Bars represent the positions of the characteristic diffraction peaks of bulk rutile and anatase.

Further, the scrolling and unscrolling of these TiO_2 nanostructures, along with the accompanying phase transitions, was found to be reversible. Increasing the pH of the diluted solution of TiO_2 nanosheets from pH 2 to pH 11 by dialysis removes protons adsorbed on undercoordinated oxygen at-

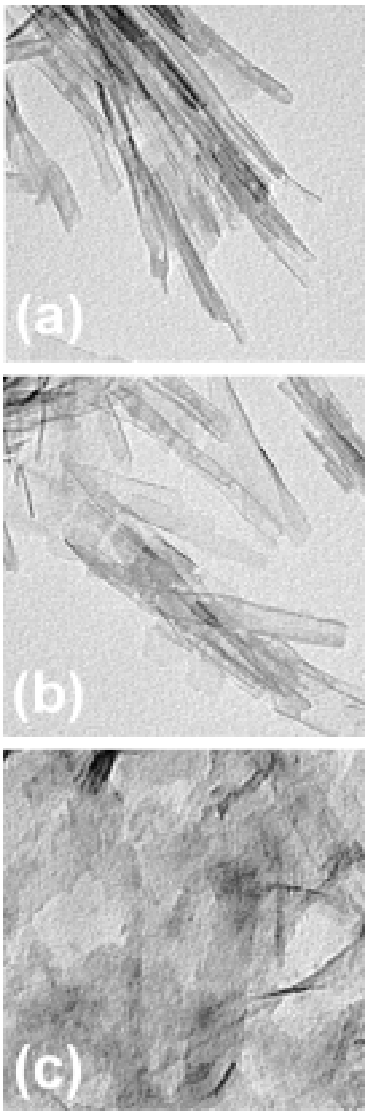

Fig. 3. HRTEM of TiO_2 (a) scrolled nanotubes (b) partially unrolled nanotubes, and (c) nanosheets. The nanotubes in (a) correspond to the structures at point A in Fig. 4, (b) corresponds to the structure during the transition B→C in Fig. 4, and (c) corresponds to the structure at point C in Fig. 4.

oms, providing a driving force for self-coiling of the TiO_2 nanosheets and the reformation of the nanotube structure. This re-scrolling re-established the anatase crystalline structure, layer thickness, and spacing of original hydrothermally generated nanotubes. A detailed account of the synthesis and characterization of these nanostructures is contained in reference [32], and an example of fully scrolled nanotubes, partially unscrolled nanotubes and completely unscrolled rutile nanosheets are shown in Figs. 3a, 3b and 3c, respectively.

At first glance, these results (with the anatase nanotubes existing in alkaline, and the rutile nanosheets existing in acid) appear completely at odds with the predictions of the theoretical model described above. However, if the free energy of anatase and rutile is plotted as a function of the surface-to-volume ratio (shown in Fig. 4), the various structural transitions can be explained by following the sequence of points indicated as A, B, C and D.

At point A, anatase nanotubes with a surface-to-volume ratio of ~0.3 nm^{-1} exist in conditions representative of alkaline solutions. Changing the pH to conditions representative of acidic conditions causes hydrogenation of the undercoordinated surface which induces a phase transition (A→B), since at this low surface-to-volume ratio the lowest energy phase is rutile. This is followed by the unscrolling of the nanotubes (B→C) into nanosheets with a much higher effective surface-to-volume ratio of ~2.2 nm^{-1}. The change of adsorbates to represent alkaline conditions induces the reverse phase transition (C→D). This is followed by the scrolling of the nanosheets (D→A) and a decrease in the effective surface-to-volume ratio to that of the nanotubes once more.

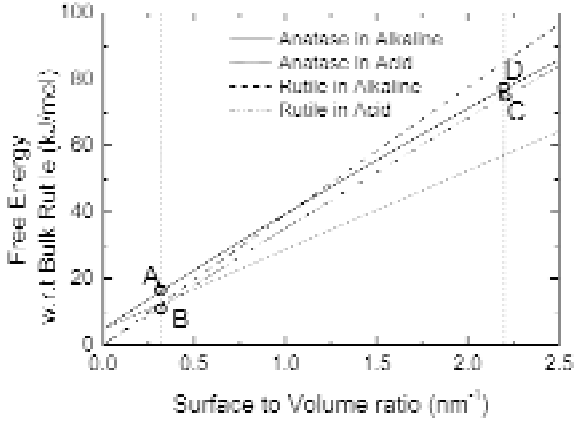

Fig. 4. Schematic representation of the free energy of rutile and anatase in acid and alkaline conditions, with respect to bulk rutile. The anatase–to–rutile (A→B) and rutile–to–anatase (C→D) phase transitions are induced by the addition of hydroxyl ions or protons; whereas the structural transitions B→C and D→A are induced by unscrolling and scrolling of nanotubes, respectively. The vertical lines at a surface-to-volume ratio of ~0.3 and ~2.2 nm^{-1} (to guide the eyes) indicate the approximate values of the surface-to-volume ratio for the nanotubes and nanosheets, respectively.

This scheme is made possible since the phase transition point for anatase and rutile in conditions representative of both acid and alkaline solutions lie between the effective surface-to-volume ratios of the scrolled nanotubes and nanosheets. Because of these phase transformations, both anatase and rutile may exist in a metastable state (at A and C, respectively) until perturbed. The opportunity for the phase transformation to occur exists only at the stages A→B and C→D, where the change in surface chemistry provides a driving force for the transition.

5. CONCLUSIONS

A number of important conclusions may be drawn from this study. By using a thermodynamic model and surface energies and surface tension calculated for anatase and rutile surfaces terminated by adsorbates with varying fractions of hydrogen and oxygen [20], we have shown that the phase stability of TiO_2 nanoparticles is highly dependent on surface chemistry [31]. It is clear from the results that anatase nanoparticles are stabilized by surface adsorbates containing a large fraction of hydrogen, whereas rutile nanoparticles are stabilized by surface adsorbates containing a large fraction of oxygen.

As a consequence of this dependence of the anatase–to–rutile phase transition on surface adsorbates, our model predicts that nanoscale phase transitions may be induced by changing the chemistry on the surfaces. Although unusual, evidence of such a phase transition is described, where anatase nanotubes are found to unscroll and transform into rutile nanosheets when the pH of the solution is changed. Such results suggest new avenues for the control and manipulation of the shape and phase of TiO_2 at the nanoscale.

ACKNOWLEDGEMENTS

This work was supported by the U.S. Department of Energy, Office of Basic Energy Sciences, under contract no.W-31-109-ENG-38.We would like to acknowledge the work of Xiaobing Zuo for the SAXS/WAXS results, and Jon Hiller of the the Argonne National Laboratory Electron Microscopy Collaborative Research Center for the HRTEM.

REFERENCES

[1] E. C. Scher, L. Manna and A. P. Alivisatos // *Phil. Trans. R. Soc. Lond. A.* **361** (2003) 241.

[2] S. Link and M. A. El-Sayed // *Annu. Rev. Phys. Chem.* **54** (2003) 331.

[3] T. Rajh, J. M. Nedeljkovic, L. C. Chen, O. Poluektov and M. C. Thurnauer // *J. Phys. Chem. B* **103** (1999) 3515.

[4] W. F. Zhang, M. S. Zhang, Z. Yin and Q. Chen // *Appl. Phys. B* **70** (2000) 261.

[5] T. Sugimoto, K. Okada and H. Itoh // *J. Colloidal. Int. Sci.*, **193** (2003) 140.

[6] A. Pottier, S. Cassaignon, C. Chaneac, F. Villain, E. Tronc and J.-P. Jolivet // *J. Mater. Chem.* **13** (2003) 877.

[7] T. Sugimoto, X. Zhou and A. Muramatsu // *J. Colloidal. Int. Sci.* **259** (2003) 43.

[8] T. Sugimoto, X. Zhou and A. Muramatsu // *J. Colloidal. Int. Sci.* **259** (2003) 53.

[9] H. Yin, Y. Wada, T. Kitamura, T. Sumida, Y. Hasegawa and S. Yanagida // *J. Mater. Chem.* **12** (2002) 378.

[10] Y. Li, T. White and S. H. Lim // *J. Solid State Chem.* **77** (2004) 1372.

[11] M. Sugiyama, H. Okazaki and S. Koda // *Jpn. J. Appl. Phys.*, **41** (2002) 4666.

[12] Y. Gao and S. A. Elder // *Mater. Lett.* **44** (2000) 228.

[13] A. Chemseddine and T. Mortiz // *Eur. J. Inorg. Chem.* (1999) 235.

[14] R. L. Penn and J. F. Banfield // *Geochimica et Cosmochimica Acta.* **63** (1999) 1549.

[15] A. Zaban, S. T. Aruna, S. Tirosh, B. A. Gregg and Y. Mastai // *J. Phys. Chem. B* **104** (2000) 4130.

[16] T. Sugimoto, X. Zhou and A. Muramatsu // *J. Colloidal. Int. Sci.* **252** (2002) 339.

[17] H. Zhang, R. L. Penn, R. J. Hamers and J. F. Banfield // *J. Phys. Chem. B* **103** (1999) 4656.

[18] T. Sugimoto and X. Zhou // *J. Colloidal. Int. Sci.* **252** (2002) 347.

[19] T. Rajh, L. X. Chen, L. Lucas, T. Liu, M. C. Thurnauer and D. M. Tiede // *J. Phys. Chem. B* **106** (2002) 10543.

[20] A. S. Barnard, P. Zapol and L. A. Curtiss // *Surf. Sci.* **582** (2005) 173.

[21] A. S Barnard and P. Zapol // *J. Chem. Phys.* **121** (2004) 4276.

[22] The experimental free energies of formation of anatase (rutile) $\Delta_f G_A^0$ ($\Delta_f G_R^0$) taken from the JANAF tables have been applied here, such that $\Delta_f G_A^0$ = -9.491471·10^{-2} mJ/mol ($\Delta_f G_R^0$ = -9.539962·10^{-2} mJ/mol). M. W. Chase, C. A. Davies, J. R. Downey, D. J. Frurip, R. A.

McDonald and A. N. Syverud, *J. Phys. Chem. Ref. Data* **14** (Suppl. 1) (1985) 1680.
[23] A. S. Barnard and P. Zapol // *Phys. Rev. B* **70** (2004) 235403.
[24] P. Vinet, J. H. Rose, J. Ferrante and J. R. Smith // *J. Phys: Condens. Matter.* **1** (1989) 1941.
[25] U. Diebold // *Surf. Sci. Rep.* **48** (2003) 53.
[26] M. R. Hoffmann, S. T. Martin, W. Choi and D. W. Bahnemann // *Chem. Rev.* **95** (1995) 69.
[27] M. C. Thurnauer, T. Rajh and D. M. Tiede // *Acta. Chem. Scan.* **51** (1997) 610.
[28] Y. Nakaoka and Y. Nosaka // *J. Photochem. Photobio. A* **110** (1997) 299.
[29] S. H. Szczepankiewicz, J. A. Moss and M. R. Hoffmann // *J. Phys. Chem. B* **106** (2002) 7654.
[30] T. Kasuga, M. Hiramatsu, A. Hoson, T. Sekino and K. Niihara // *Adv. Mater.* **11** (1999) 1307.
[31] A. S. Barnard and L. A. Curtiss // *Nano Letters* (2005), in press.
[32] Z. V. Saponjic, N. Dimitrijevic, D. Tiede, A. Goshe, X. Zuo, L. Chen, A. S. Barnard, P. Zapol, L. A. Curtiss and T. Rajh // *Adv. Mater.* **17** (2005) 965.